Structural Engineering and Mechanics, *Vol. 72, No. 4 (2019) 421-432*
DOI: https://doi.org/10.12989/sem.2019.72.4.421

Structural noise mitigation for viaduct box girder using acoustic modal contribution analysis

Liu Linya[1], Jialiang Qin[1], Yun-Lai Zhou*[2], Rui Xi[1] and Siyuan Peng[1]

[1]*Engineering Research Center of Railway Environment Vibration and Noise Ministry of Education, East China Jiaotong University, Nanchang 330013, China*
[2]*Department of Civil and Environmental Engineering, National University of Singapore, 117576, Singapore*

(Received October 31, 2018, Revised May 3, 2019, Accepted June 20, 2019)

Abstract. In high-speed railway (HSR) system, the structure-borne noise inside viaduct at low frequency has been extensively investigated for its mitigation as a research hotspot owing to its harm to the nearby residents. This study proposed a novel acoustic optimization method for declining the structure-borne noise in viaduct-like structures by separating the acoustic contribution of each structural component in the measured acoustic field. The structural vibration and related acoustic sourcing, propagation, and radiation characteristics for the viaduct box girder under passing vehicle loading are studied by incorporating Finite Element Method (FEM) with Modal Acoustic Vector (MAV) analysis. Based on the Modal Acoustic Transfer Vector (MATV), the structural vibration mode that contributes maximum to the structure-borne noise shall be hereinafter filtered for the acoustic radiation. With vibration mode shapes, the locations of maximum amplitudes for being ribbed to mitigate the structure-borne noise are then obtained, and the structure-borne noise mitigation performance shall be eventually analyzed regarding to the ribbing conduction. The results demonstrate that the structural vibration and structure-borne noise of the viaduct box girder mainly occupy both in the range within 100 Hz, and the dominant frequency bands both are [31.5, 80] Hz. The peak frequency for the structure-borne noise of the viaduct box girder is mainly caused by 16th and 62th vibration modes; these two mode shapes mainly reflect the local vibration of the wing plate and top plate. By introducing web plate at the maximum amplitude of main mode shapes that contribute most to the acoustic modal contribution factors, the acoustic pressure peaks at the field-testing points are hereinafter obviously declined, this implies that the structure-borne noise mitigation performance is relatively promising for the viaduct.

Keywords: box girder viaduct; structure-borne noise; vehicle-viaduct coupling; acoustic modal contributor; FEM

1. Introduction

The noise in high-speed railway (HSR) system has been a hotspot in both research committees and actual engineering firms because of its negative effect in the safety and in-service comfort of the HSR. The noise in HSR has various forms as shown in Fig. 1, such as catenary induced noise, aerodynamic noise, carriage-borne interior noise, wheel-rail (vehicle viaduct) induced noise because of their interaction, structure-borne noise from the viaduct and so on (Dai *et al.* 2019). Among all these kinds of noises, the structure-borne noise from the viaduct serves as an essential role especially when considering its nearby influence and its wide use in long HSR system even more than 90% of the full length in Guangzhou-Zhuhai intercity railway (He *et al.* 2017), which shall probably affect the daily lives of the residents and potential institutions.

The structure-borne noise mitigation for the viaducts has been an essential research focus due to the harmful noise consequences to the civil engineering, mechanical engineering and aerospace engineering (Gille *et al.* 2017),

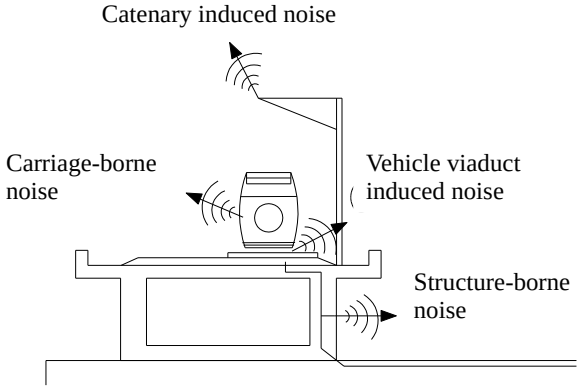

Fig. 1 Typical noises induced in the HSR system

therefore leading to influence in their designs such as in bridge preliminary design with finite element (FE) model analysis (Cao *et al.* 2017). The structure-borne noise can decline the satisfaction rate in the airplanes, auto vehicles and submarine vehicles. In terms of civil engineering, the structure-borne noise induced by the ambient uncertainties and moving loads shall enable the related structures to undergo local and/or global vibration, and such vibration shall probably lead to the degradation of in-service life (Gille *et al.* 2017, Foglar and Goringer 2013, Thota and Wang 2017, Dijckmans *et al.* 2015). The reason hidden behind is that the local vibration shall induce the local stress

*Corresponding author, Ph.D.
E-mail: zhouyunlai168168@gmail.com

ISSN: 1225-4568 (Print), 1598-6217 (Online)

concentration, which will probably generate fatigue crack, and such fatigue crack will decline sharply the service life of the vehicles, for instance, the local vibration in the bogie shall induce fatigue crack. Hereinafter, certain structure-borne noise mitigation performs significantly in rail transportation systems (Dijckmans *et al.* 2015). One option is to mitigate the noise resource such as the vibration, and to use floating slab especially damping pad floating slab can provide promising potential in mitigating the vibration in the rail transit (Liang *et al*. 2019).

The structural acoustic and dynamic analysis can date back to the integrated approach of finite element method (FEM)/boundary element method (BEM) (Kopuz *et al.* 1996), where the application of FEM and BEM in predicting the dynamic and acoustic behavior is justified. The engine noise radiation is computationally analyzed by employing acoustic transfer vectors (ATVs) and modal acoustic transfer vectors (MATVs) in the frequency domain (Gerard *et al.* 2002); more in-depth dynamic analysis for engines can refer to (Siano *et al*. 2018, Armentani *et al*. 2016, 2018); vibro-acoustic prediction in the low-frequency to mid-frequency range is implemented with numerical study and experimental verification to demonstrate the developed FEM-BEM methodology can employ the MATV algorithm in resolving large-scale problems (Citarella *et al.* 2007). The MATV methodology initiates from the conventional modal analysis in mechanical engineering, a discussion for jointed structures can refer to (Quinn 2012). On the other hand, ATV has also been applied for talker location discrimination combining by utilizing multiple kernel learning and also hidden Markov model (Takashima *et al.* 2013a, b); in addition, the transfer matrix method has also been successfully applied in vibration analysis for pipeline (Liu *et al.* 2013).

As to rail transportation system, vibro-acoustic is a typical and essential issue and has been analyzed with various approaches. Sadri and Younesian (2015) studied the structure-borne noise of a rail vehicle cabin under random excitation by utilizing Durbin's numerical Laplace transform inversion algorithm. In the investigation of a vibrating steel bridge for the transient acoustic radiation under passing traffic loading, Zhang *et al.* (2015a) investigated the sound pressure level and the structure-borne noise radiation mechanism by minimizing the interaction force between the analytical and experimental results. Vibro-acoustic analysis for the acoustic-structure interaction of the flexible structures under acoustic excitation is investigated with BEM-FEM (Djojodihardjo 2015). Apart from the above approaches, the MATV method illustrated above has also been extensively employed in analyzing the vibro-acoustic problems; for instance, Li *et al.* (2014) investigated structure-borne low-frequency noise from the concrete rail transit bridges using 2.5-dimensional method to compute the MATV for assessing the sound pressure. The irregularity at the contacting surface between wheels and rails shall form excitation when the vehicle passes the viaduct, which shall generate vibration in all components of the HSR system such as carriage, rail, foundation and so on, and also high-frequency radiation noise in the frequency range [800, 2000] Hz, and the corresponding vibration in the viaduct will result in the generation of structure-borne noise. Certain structure-borne noise in the viaducts mainly occupies in the range of [20, 200] Hz low frequency noise (Liu and Song 2002, Zhang *et al.* 2013a). Certain frequency range noise has low attenuation coefficient, conventional noise barrier could not effectively lessen certain noise, which is detrimental to human beings, related investigations can refer to Ngai and Fng (2002), Gao *et al.* (2010), Werning *et al.* (2001) and Møller and Pedersen (2011). With the development of HSR, the application of viaducts has been increased abroad in long distance HSR system since it can reduce the use of land (He *et al.* 2017); the complaints for the low frequency noise are furthermore expanding accordingly (Crockett and Pyke 2000, Werning *et al.* 2001). All these negative affairs request for critical solution to the mitigation of both acoustic and dynamic vibration for the viaducts.

The introduction of ribbing plate to improve the structural stiffness is a solution to reduce the structure-borne radiation noise. Xie *et al.* (2008) investigated the acoustic characteristics of introducing rib to the simply supported cylinder ferroconcrete shell, and claimed that proper ribbing can mitigate the structure-borne acoustic sound pressure level. The acoustic influence of adding ribbing to cylinder shell under water was studied in (Harari and Sandman 1990, Liao *et al.* 2009). Han *et al.* (2012) introduced horizontal rib to channel girder section, and claimed that the adoption of horizontal rib can effectively lessen the structural noise, the use of full section rib is better than solely applying the rib in the middle intensely, which furthermore suggested that the appropriate rib position could potentially affect the eventual noise mitigation performance.

In the structural acoustic field optimal design for the viaduct-like structures to reduce the corresponding structure-borne noise, the determination of the positions for adding rib plates has to be updated considering the noise mitigation manifestation, the economic cost, and the environmental affection. However, up to now, in viaduct structure-borne noise mitigation, few studies can be found on ribbing plate placement optimization in acoustic field optimal design.

This study took the viaduct box girder as investigation target, and developed a methodology for precisely locating the optimal position. FEM and MATV method are hereinafter employed to investigate the vibration and acoustic characteristics of the viaduct box girder under passing vehicle loadings, then MATV is then utilized to identify the structural mode that contributes most to the structure-borne acoustic noise responses of the viaduct box girder. In accordance to the corresponding mode shapes, the positions of adding rib are hereinafter determined; finally the structure-borne acoustic noise mitigation manifestation before and after adding rib is analyzed.

2. Theoretical background

2.1 Modal Acoustic Transfer Vector (MATV)

Under small pressure perturbation, the acoustic equation can be considered to be linear, and by using discrete boundary element method (DBEM), the linear relation

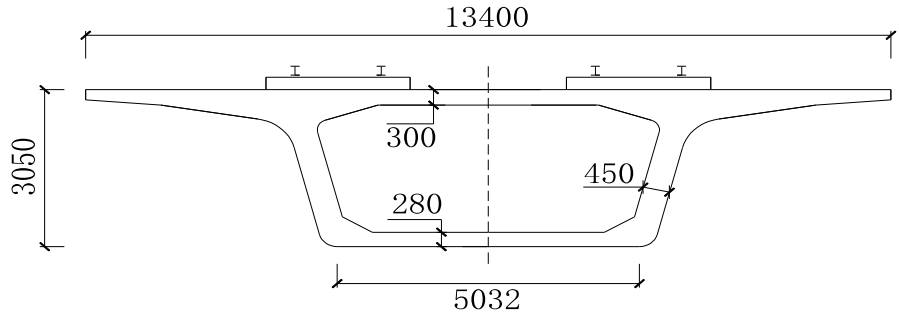

Fig. 2 The dimensions for the box girder section (unit: *mm*)

between input (the viaduct surface vibration) and output (acoustic pressure at certain acoustic field location) can be then determined, and the acoustic pressure in the field can be illustrated as

$$p(\omega) = \{A(\omega)\}^T\{v(\omega)\} \tag{1}$$

where $A(\omega)$ represents the acoustic transfer vector (ATV), which is the structural physical characteristic, depending on the material property like density, sound velocity in the medium, structural geometry and so on. ATV can be considered as the acoustic pressure at certain acoustic field location generated by the unit velocity of a certain element or node at certain frequency. In order to obtain clear understanding for ATV, following parts aim to explain the acoustic modal analysis from conventional modal analysis.

In terms of structural vibration, the structural dynamic displacements can be obtained by mode superposition method, expressed as

$$\{u\} = \Omega \cdot \{MCF(\omega)\} \tag{2}$$

where $\{u\}$denotes the structural displacement, Ω represents the structural modal matrix, $\{MCF(\omega)\}$ illustrates the modal contribution factor (MCF).

By projecting the structural displacement vector into the normal direction of the structural surface, thereafter the structural vibration velocity at the normal direction can be expressed as

$$v_n = j \cdot \omega \cdot \Omega_n \cdot \{MCF(\omega)\} \tag{3}$$

where Ω_n depicts the sub-vector matrix at the normal direction of structural surface of the structural vibration modes, and the acoustic pressure is computed as

$$p(\omega) = \{ATV\}^T \cdot j \cdot \omega \cdot \Omega_n \cdot \{MCF(\omega)\} = \{MATV(\omega)\}^T \cdot \{MCF(\omega)\} \tag{4}$$

where $\{MATV\}^T$ represents the conjugate of the MATV, of which the physical meaning is that the acoustic pressure induced by unit mode response at certain frequency at one element or node, $\{MATV\}^T$ can be determined by

$$\{MATV(\omega)^T\} = j\omega \cdot \Omega_n \cdot \{MCF(\omega)\} \tag{5}$$

Eq. (4) can also be written as

$$p_s = \sum_{i=1}^{N} (p_{si} + p_{si}^*) \tag{6}$$

where $p_{si} = \{ATV(w)\}^T \cdot j \cdot w \cdot W_{ni} \cdot MCF_i(w)$ represents the field acoustic pressure induced by the i^{th} structural vibration mode. p^* means the conjugate of the p. N means the modal order considered. p_s means the acoustic pressure at s. From Eq. (6), MATV can determine the acoustic field pressure, and also can identify the structural vibration mode that contributes most to the field sound pressure, and this shall provide the theoretical fundamental for the viaduct structure-borne noise mitigation.

3. Viaduct box girder model

3.1 FE model for viaduct box girder

This study takes the viaduct box girder from certain HSR system as research target, and the section dimension is illustrated in Fig. 2. The viaduct has 32.5 *m* in length, the span is 31.5 *m*, the height for the box girder is 3.05 *m*, and the width is 13.4 *m*, the thickness of the top plate is 0.3 *m*, the thickness for the web is 0.45 *m*, the bottom plate thickness is 0.28 *m*. This model ignores the effect of the supporters and the foundation, and the viaduct is considered as simply supported.

This study employs plate element to model the viaduct box girder, the slab track, the CA mortar, and the concrete foundation are modeled with solid element, the rail fasteners utilize spring damping element in modeling, the rail is modeled with beam element.

The elements and parameters that were taken into account in the FE model for the rail and viaduct are shown in Table 1, and the built FE model is illustrated in Fig. 3.

3.2 Acoustic model for the viaduct box girder

In terms of FE acoustic model, the maximum element size in FEM cannot exceed the 1/6 of the minimum wavelength of calculation frequency, depicted as

$$L \leq \frac{c}{6f_{max}} \tag{7}$$

where c=340 *m*/*s* denotes the sound speed in air, the maximum meshing size of L for acoustic model for box girder is 0.25 *m*. With Equation (7), the maximum

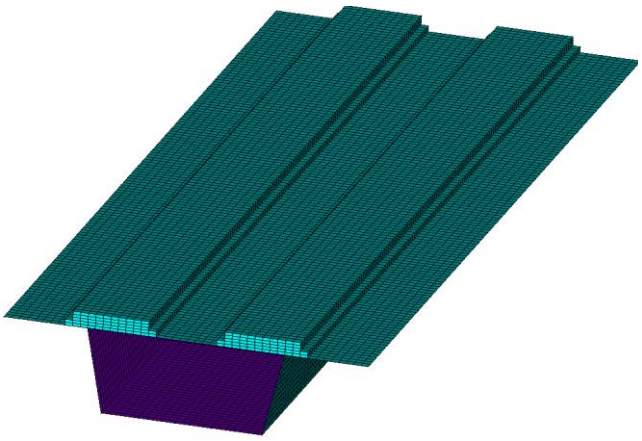

Fig. 3 The FE model for the viaduct box girder

Table 1 Elements and material properties for the FE model of the viaduct box girder

0	Element	Material properties		
		Young's modulus	Density (kg/m^3)	Poisson's ratio
Viaduct	SHELL63	35 GPa	2500	0.2
Base	SOLID45	33 GPa	2500	0.2
CA mortar	SOLID45	0.8 GPa	1300	0.2
Slab track	SOLID45	35 GPa	2500	0.2
Fastener	COMBIN14	Stiffness: 60 *kN/mm*, damping: 10^4 *N.s/m*		
Rail (CHN60)	BEAM188	210 GPa	7830	0.3

calculation frequency can be up to 226 Hz. The viaduct structure-borne noise mainly behaves in the low frequency, less than 200 Hz, and then the acoustic model fulfills the accuracy requirements in computation. The FE acoustic model for the viaduct box girder is depicted in Fig. 4.

4. The vibration and acoustic analysis for the viaduct box girder

4.1 The solver and loading of the vehicle-wheel coupling system

Track irregularity induces the interaction between the wheel and the rail, which shall further perform as excitation acting between the wheel and the rail, which is the source for viaduct box girder vibration. Thereafter, before predicting the structural vibration and structure-borne noise of the viaduct box girder, it is necessary to understand the interaction force between the wheel and the rail. Simpack multi-body dynamic and ANSYS software are utilized to construct the vehicle-viaduct coupling model expressed in Fig. 5(a) with taking the vertical contacting force into account to further compute the wheel-rail interaction force.

This study utilizes two carriages of CRH2 depicted in Fig. 5(b) to model the loading, each carriage consists of two bogies and four wheel pairs, the calculation speed is 200 *km/h*, the integration time interval is 0.002227 *s*, only the

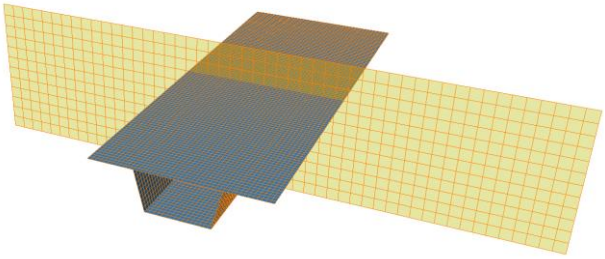

Fig. 4 The acoustic model for the viaduct box girder

right side track of the dual track model is considered with passing high-speed trains in computation.

As to the track irregularity spectrum, since no standard spectrum in China exists for investigation, Germany low interference spectrum, which is similar to Chinese track irregularity spectrum, is taken as track irregularity excitation for the viaduct-vehicle coupling system. The wheel-rail vertical acting force can be then obtained by resolving the vehicle-viaduct coupling system. Fig. 6 shows the vertical acting force at the first pair of wheels. Since this German low interference spectrum is measured from engineering, this spectrum has already included the uncertainties from the real engineering.

4.2 Structural vibration analysis for the viaduct box girder

In order to study the dynamic characteristics of the viaduct box girder under vehicle loading, the points at top (marked as 'A' in Fig. 7) and bottom (marked as 'B' in Fig. 7) plates at the middle-span section are considered as targets for vibration responses analysis, depicted in Fig. 7.

With the wheel-rail acting force as excitation for the viaduct box girder, the vibration responses of the viaduct can be obtained with FEM. By using merely the right side loading, two carriages are simplified to be eight-point loads, and the loading interval is 0.002227 s. Fig. 8 demonstrates the acceleration responses of the viaduct box girder for all testing points. Fourier transform was hereinafter applied for spectrum analysis, and further the acceleration responses are transferred to one-third-octave curves for frequency domain analysis. Fig. 9 expresses the excitation force, and acceleration response versus one-third-octave frequency for the mid-span point at the top and bottom plates.

In Fig. 9, for the testing points at both top plate location "A" and bottom plate location "B", the vibration responses mainly ranged within 100 Hz, and the viaduct vibration responses principally ranged in the frequency range [31.5, 80] Hz, the peak frequencies are 63 Hz and 80 Hz, respectively, the corresponding peak accelerations are 98.2 dB and 94.6 dB, respectively. This finding agreed well with the previous investigation findings (Zhang *et al.* 2015b), which proved the feasibility of the proposed model in structural dynamic investigation.

4.3 Acoustic radiation characteristic for viaduct box girder

In order to determine the structure-borne noise analysis for the viaduct box girder with moving high-speed trains,

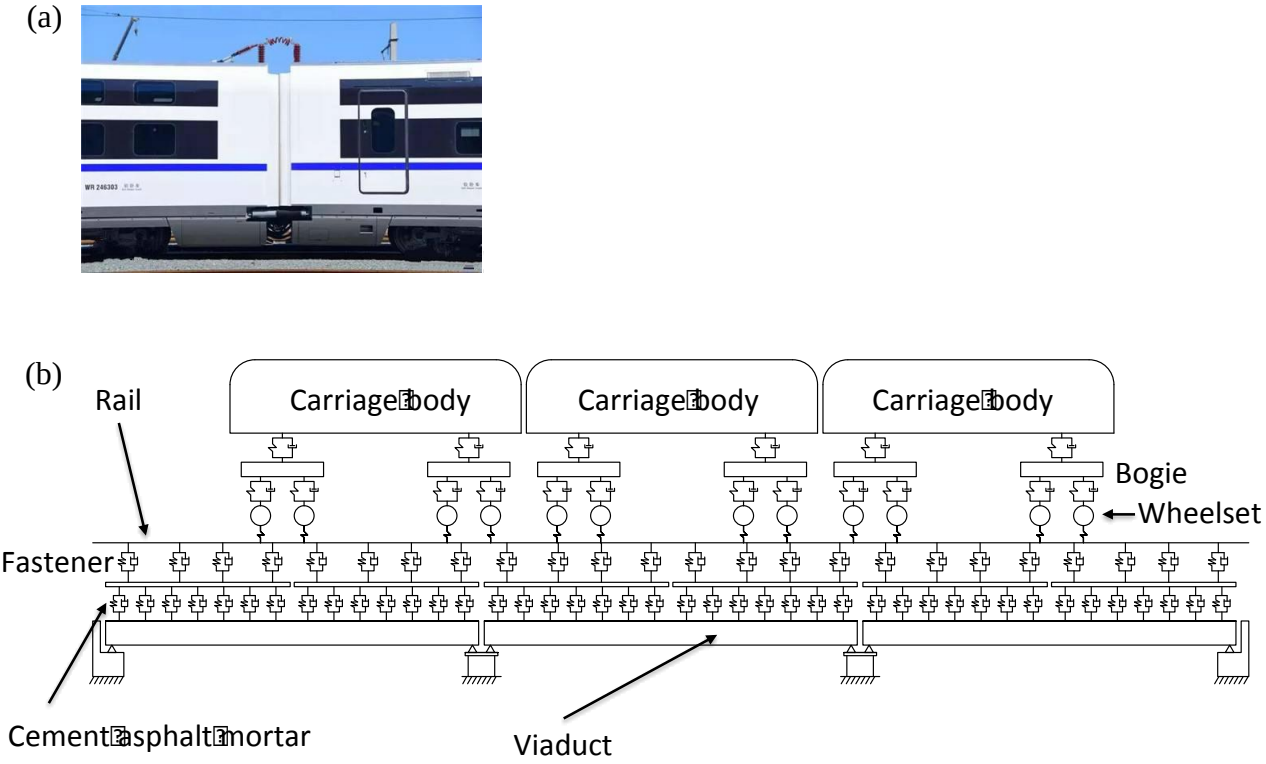

Fig. 5 (a) Vehicle-track coupling dynamics model; (b). CRH2 carriage

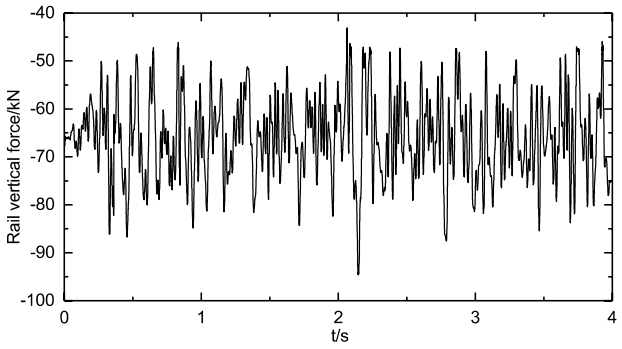

Fig. 6 The vertical acting force at the first pair of wheels

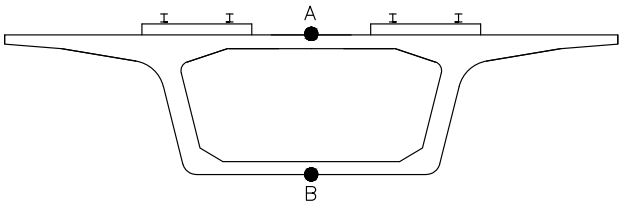

Fig. 7 The studying points for vibration analysis.

the field-testing points are then chosen with reference points varying distances in the acoustic field, detailed in Fig. 10. The field-testing points D1-D4 locate vertically under the mid-span section of the viaduct, the field-testing points D5-D9 locate with 1.2 *m* higher than the land surface. The field-testing points D9-D13 locate vertically with 3 *m* far from the middle span of the box girder. The detailed information for all positions is shown in the schematic diagram in Fig. 10. The reason for such field-testing points design relies on the fact that this design serves as the minimum measuring points design but with full information in estimating the acoustic field.

Current A-weight evaluation indicator alleviates more for low frequency noise. For accurately evaluating the low frequency structure-borne noise, this study employed un-weighted linear sound pressure level analysis. Fig. 11 displayed the one-third-octave sound pressure lines for all field-testing points.

From the one-third-octave linear sound pressures and their amplitudes at the center frequency shown in Fig. 11, the sound pressure levels at the field-testing points D1-D3 decreased as the distance to the bottom plate enlarged; the sound pressure at the field-testing point D4 is greater than that at the field-testing point D3, due to that the field-testing point D4 is closer to land surface, which completely reflected the structure-borne noise and amplified the sound pressure at the field-testing point D4; the sound pressure at the field-testing points D5-D8 decreased as the horizontal distance from the middle span section of the box girder increased; and the increase from the same distance interval became increasingly smaller. As to the field-testing points D9-D13 with 3 *m* in horizontal distance to the middle span section of the box girder, the sound pressure levels decreased as their heights of the field-testing points from the land surface increased in the frequency range less than the center frequency of 25 Hz; however, for the frequency range larger than the center frequency of 25 Hz, the sound pressure levels changed without clear rules. All the structure-borne noises from the field-testing points D1-D13 principally ranged in the frequency range [31.5, 80] Hz, and

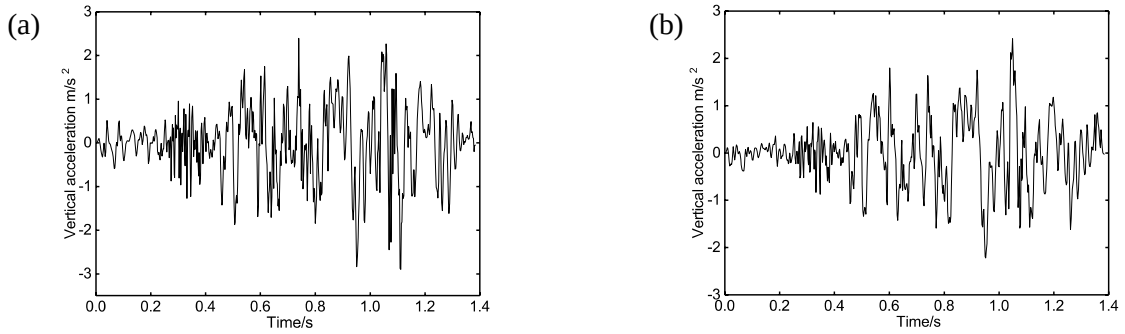

Fig. **8**. Vertical accelerations for the middle-span points at (a) "A" in Fig. 7; (b) "B" in Fig. 7.

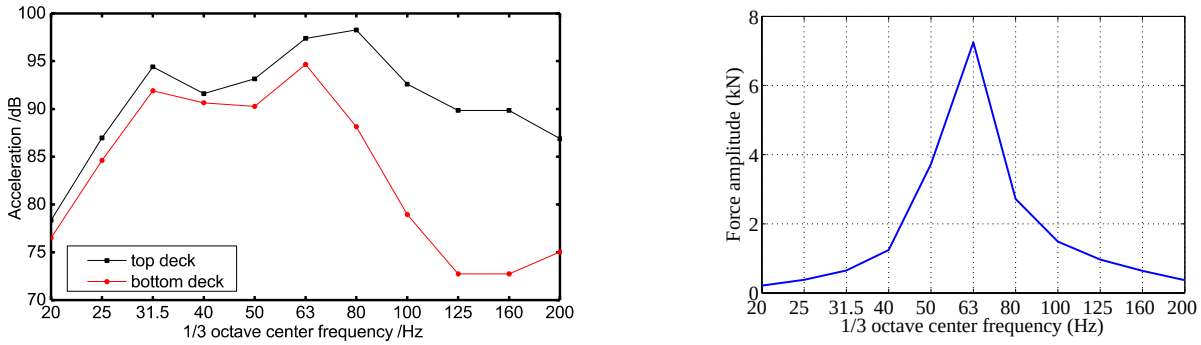

(a) (b)

Fig. 9 The force and acceleration response: (a). the acceleration of the field-testing point at "A" and "B"; (b). the force amplitude in frequency domain

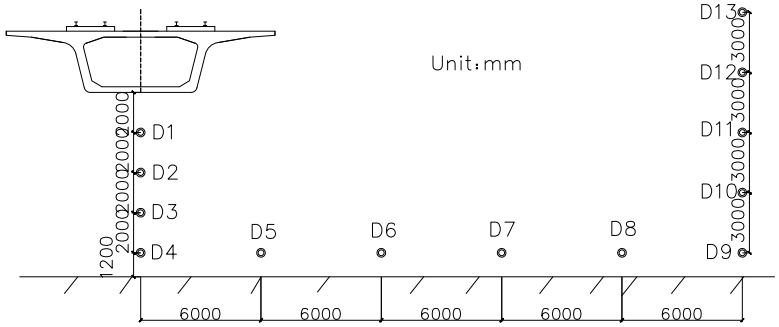

Fig. 10 The schematic diagram of the viaduct box girder model and the field-testing points distribution

have peak values in the frequency band around 31.5 Hz, 63 Hz, and 80 Hz, respectively; such finding affirms the concluding remarks in (Zhang *et al.* 2015b), and also proved that the MATV method shall be capable of applying for computing the viaduct structure-borne noises.

In the center frequencies bands around 31.5 Hz, 63 Hz, and 80 Hz, respectively, the viaduct displays principally with local vibration at the surface plates, and the peak frequency of the excitation also locates in this range (shown in Fig. 9b), which easily generated the resonance, and made the structural noises comparatively larger. This agreed well with the previous experimental tests in (Li *et al.* 2013, Zhang *et al.* 2013b). As discussed above, it shall be indispensable to raise effective solutions to mitigate the structure-borne noises at these dominant frequency bands.

For all the field-testing points D1-D13, the sound pressures mainly demonstrated comparatively larger sound. pressure peaks at 31.5 Hz and 80 Hz, respectively; then Fig 12 (a) and (b) illustrated the two dimensional acoustic field for the middle-span section of the viaduct at 31.5 Hz and 80 Hz, respectively. From Fig. 12 (a) and (b), when the frequency is low, the acoustic field directional characteristic is stronger; and as the frequency enlarged, the acoustic field distribution became complex, while the structure-borne noises directly below and above the box girder section change with high gradient at the left side as shown in Fig.12 (a) and (b), respectively. The sound pressures at the areas directly below and above the box-girder section were larger than those of other areas. In the horizontal space, the sound pressure levels decreased as the distance to the middle span section of the viaduct box girder increased. For the far acoustic field (at the field-testing points D9-D13), the sound pressure levels decreased as the height from the land surface increased.

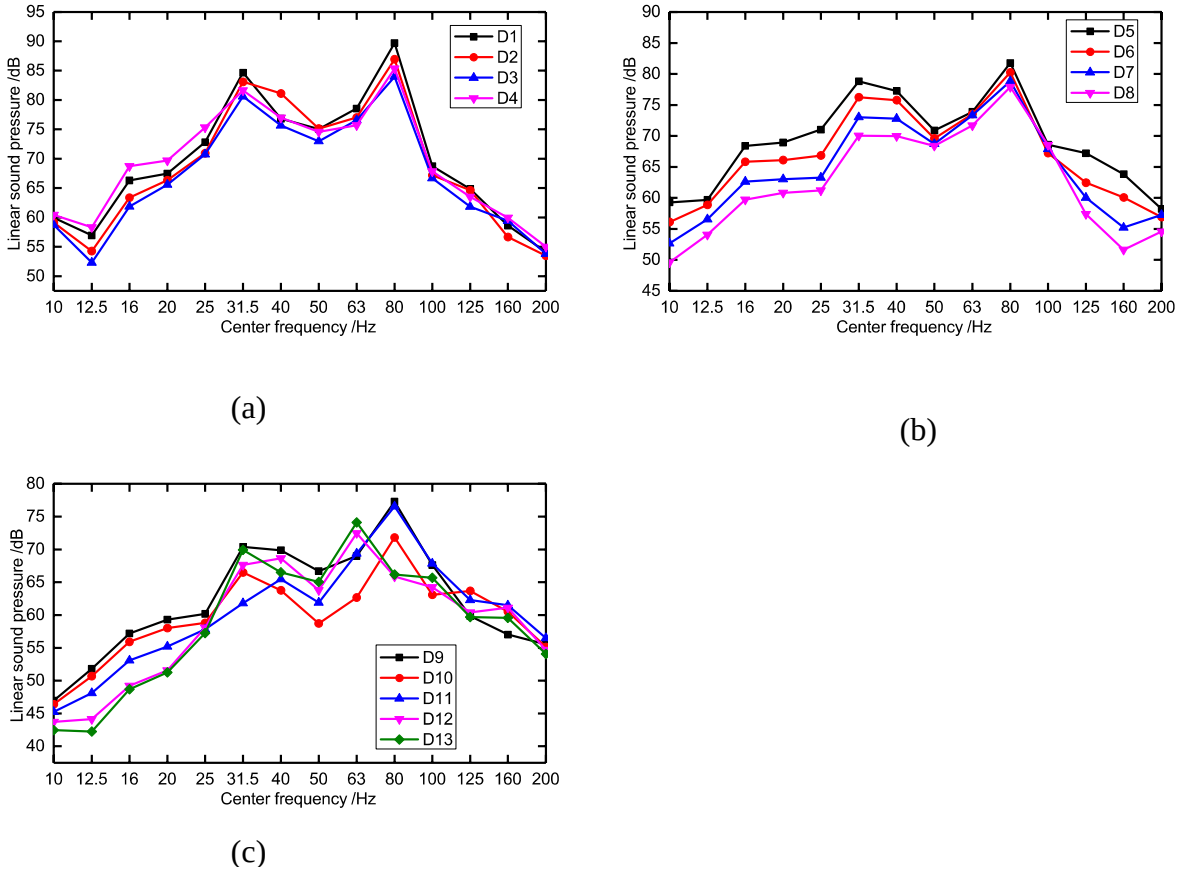

Fig. 11 One-third-octave sound pressure curves at the field-testing points: (a) D1-D4; (b) D5-D8; (c) D9-D13

5. Acoustic optimal design for the viaduct box girder

5.1 Acoustic modal contribution analysis for the viaduct box girder

In order to gain the influence of the mode shapes to the acoustic pressure peaks, acoustic modal contribution factor analysis for the viaduct box girder is hereinafter implemented via the MATV approach. The field-testing point D9 is taken into account as studied object based on the Chinese national standard: Environmental quality standard for noise (GB 3096-2008), two frequencies of 31.5 Hz and 80 Hz are considered for further investigation. Fig. 13 (a) and (b) illustrated the determined acoustic modal contributors at 31.5 Hz and 80 Hz, respectively.

In Fig. 13, although a large number of modes dedicated comparatively large to the acoustic field sound pressure peaks at the field-testing points, but not all the modes maintain the same phases in contributing to the total acoustic pressures. While the acoustic modal contribution is positive, it suggests the mode held the same phase with the total acoustic pressure, vice versa. Each mode shall contribute to the structural global response at each frequency, but not all modes behave in the same phase, if some modes behave in the same phase as the structural global response, we call such contribution to be positive; if some modes behave in the opposite phase as the structural global response, we call such contribution to be negative. The more the same structural mode phase contributed to the total acoustic pressure, the larger the acoustic pressure at the field-testing points shall be. Thereafter, the reduction of these corresponding modal vibrations shall also effectively mitigate the structure-borne acoustic noise. And if the phase is opposite from the total acoustic pressure, the increase of the structural vibration shall alleviate the total acoustic pressures at the field-testing points.

Since the MATV connects the modes with the sound pressure fields, with choosing the first three modes that made more acoustic contribution than other modal modes, Table 2 listed the consequences of the first three dominant modal modes, modal contribution and corresponding mode shape behaviors corresponding to the peak frequencies at the acoustic field-testing points.

As to Table 2, in terms of the first three dominant modes for the peak frequency at the field-testing points, these modes are 2^{nd}, 13^{th}, 16^{th}, 44^{th}, 62^{th}, and 64^{th} order. Fig. 14 displayed the mode shapes for these vibration modes. For the acoustic modal contribution analysis, it is possible to find that for the two analytical frequencies 31.5 Hz and 80 Hz at the field-testing point D9, the acoustic pressure peaks were mainly induced by the 16^{th} and 62^{th} modes, and these two modes expressed principally as the local vibrations of the wing plate and the top plate as well. In Fig. 14, the colors represent the distinct amplitudes in the mode shapes: the red means the highest amplitude, and the blue means the amplitude is zero.

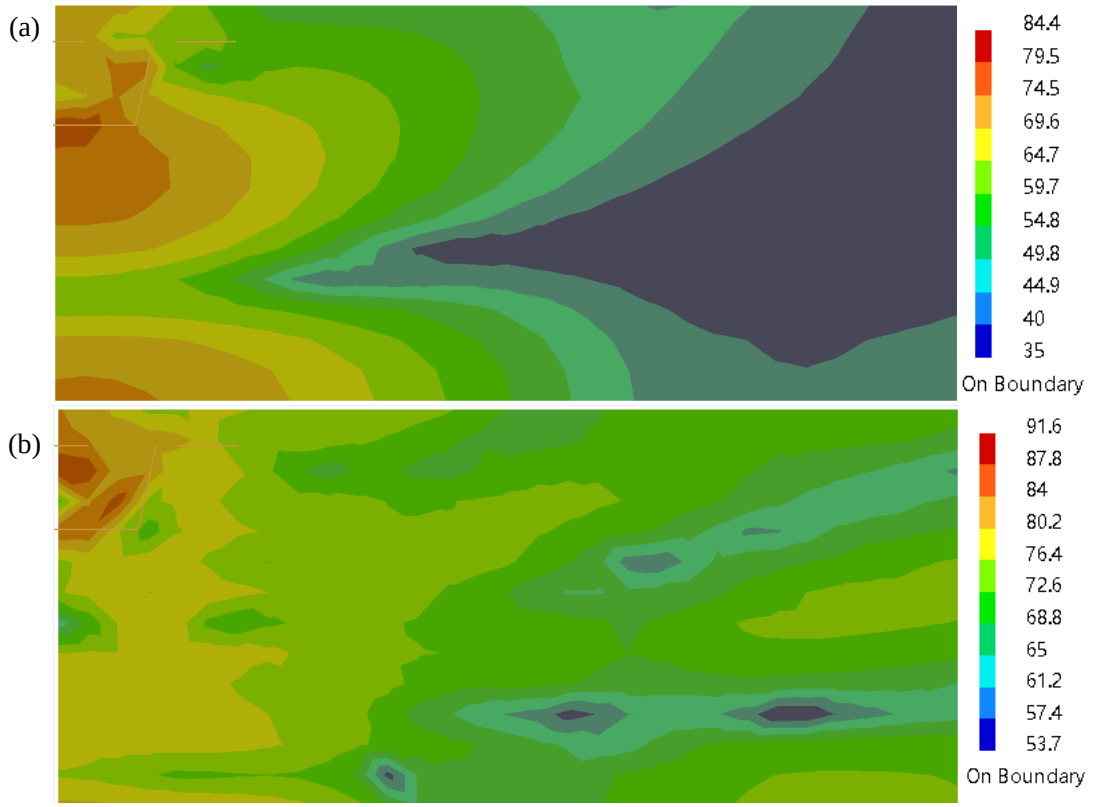

Fig. 12 Two-dimensional acoustic field at the middle span section at (a). 31.5 Hz, (b). 80 Hz, (unit: dB)

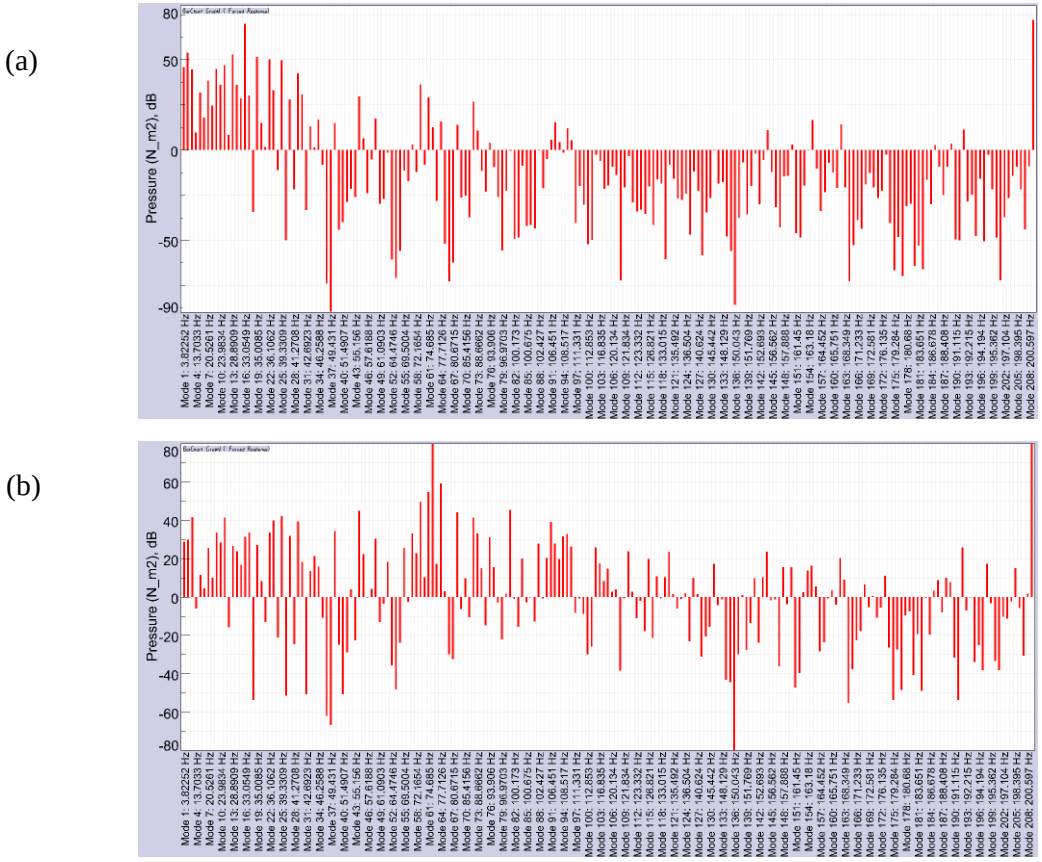

Fig. 13 The acoustic modal contribution from all modes to the field-testing point D9 at certain frequencies (a) 31.5 Hz; (b) 80 Hz

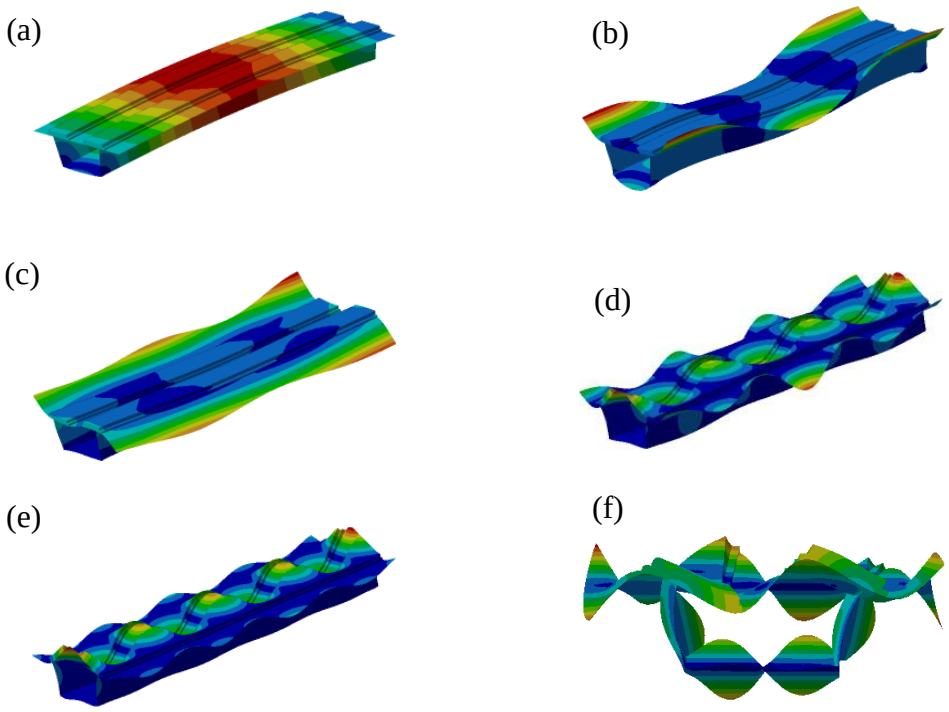

Fig. 14. Some typical mode shapes: (a) 2^{nd}; (b) 13^{th}; (c) 16^{th}; (d) 44^{th}; (e) 62^{th}; (f) 64^{th} mode shape

Table 2 First three dominant modal modes at the field-testing point D9

Mode order	Analytical frequency (Hz)	Resonant frequency (Hz)	Acoustic modal contribution (dB)	Mode shape
16		33.05	70.07	Local vibration and torsion of wing plate
2	31.5	5.787	59.83	1st vertical bending
13		28.89	52.8	Local vibration of wing plate
62		76.58	79.79	Local vibration of top plate
64	80	77.71	59.32	Viaduct plate local vibration
44		56.92	53.02	Local vibration of wing plate and top plate

5.2 Acoustic optimal design for viaduct box girder

The section discussed hereinafter aims to optimize the viaduct box girder for alleviating the structure-borne noise from the consequences of acoustic modal contribution analysis, and eventually reaches the optimal design. Taking the acoustic pressure at the field-testing point D9 as designed position for structure-borne noise mitigation, to optimize the corresponding modes through introducing rib plates to the viaduct box girder. The introduction of rib plates is capable of modifying the structural local stiffness of the plate, and reducing the local vibration, ultimately, leading to the alleviation of the structure-borne noise to the field-testing points from these modes. In summary, the mode shapes that contribute most to the structural global vibration shall be determined, and then the ribbing plates are introduced to the maximum amplitude locations of these modes to alleviate the vibration and structure-borne noise as well.

In Fig. 14, in accordance to the 16^{th} and 62^{th} mode shapes, the optimal design for the acoustic field is implemented separately to the raw model. The 16^{th} mode shape behaved primarily as the local vibration of the wing plate and the lateral bending of the viaduct; while the 62^{th} mode shape behaved mainly as the local vibration of the top plate. In regards to the 16^{th} mode shape, the local vibrations of wing plates are not symmetrical. The locations with high acoustic amplitudes primarily followed the moving direction of the vehicle on the viaduct box girder; at one side, the locations with large acoustic amplitudes are at 14.25 *m* and 31.5 *m*, respectively; while at the other side, the locations with large acoustic amplitudes are at 8.5 *m* and 29.75 *m*, respectively. Therefore, it then shall be indispensable to optimize aforementioned four locations via introducing four rib plates in the wing plates at 8.5 *m* and 14.25 *m*, respectively, and five rib plates at 29.75 *m* and 31.5 *m*, respectively.

From the 62^{th} mode shape in Fig. 14, the local vibration had comparatively uniform distribution at the dominant positions, and the positions with high amplitudes primarily followed the vehicle moving direction at the viaduct box girder at the locations 0 *m*, 3.75 *m*, 8 *m*, 12 *m*, 16.25 *m*, 20.25 *m*, 24.75 *m*, 28.75 *m*, and 32.5 *m*, respectively; and these positions requested the further optimization, and the easiest way is to introduce rib plate - one concrete plate

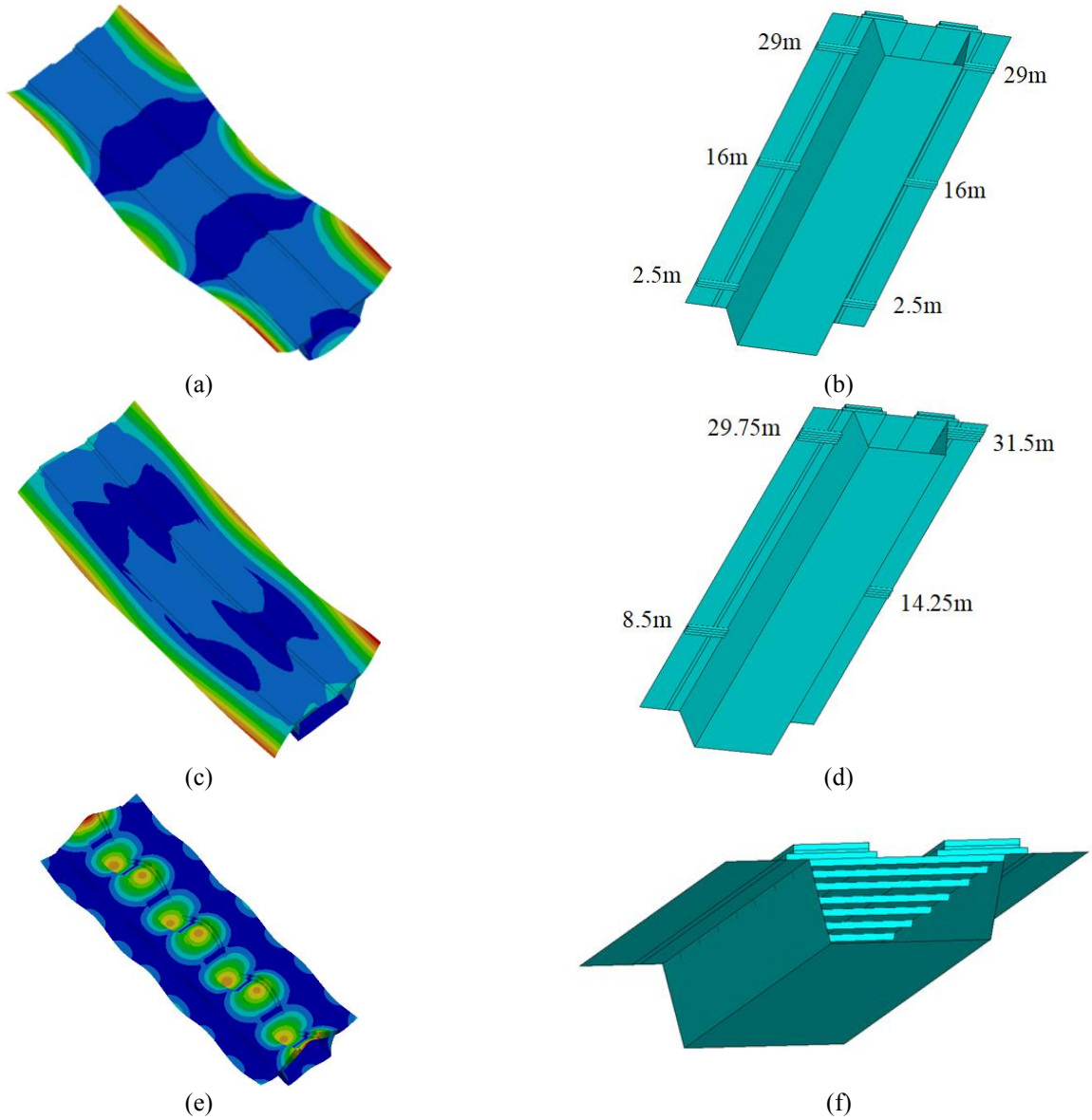

Fig. 15 Optimal design model for the viaduct box girder: (a) 13^{th} mode shape; (b) ribbing location according to 13^{th} mode shape; (c) 16^{th} mode shape; (d) ribbing location according to 16^{th} mode shape; (e) 62^{th} mode shape; (f) ribbing location according to 62^{th} mode shape

with 0.2 *m* in thickness at each aforementioned position with using the same material as the viaduct under the concern of economy cost. Hereinafter the optimized model with highlighting the ribbing plate locations is illustrated and detailed in Fig. 15. The ribbing locations are determined from the maximum amplitude in the mode shapes that contribute most to the final results.

Fig. 16 illustrated the acoustic pressure spectrums for the optimized model at the field-testing point D9. From Fig. 16, the acoustic pressure at the peak frequency evidently alleviated after taking the acoustic field optimal design. The acoustic pressure at the field-testing point D9 declined by 1.47 dB at 31.5 Hz, and reduced by 3.93 dB at 80 Hz, respectively. Distant acoustic pressure mitigation existed at the frequency 50 Hz, while for other frequencies, no obvious acoustic pressure mitigation performance could be discovered.

Fig. 17 demonstrated the comparison of the largest acoustic pressures at the field-testing points D1-D13 between the original and optimized models. Regarding to the field-testing points D1-D4 directly below the bottom plate, the maximum acoustic pressures at the field-testing points D1, D2 and D4 all are alleviated for the optimized model, and the maximum acoustic pressures declined most at the field-testing point D4 by 5.8 dB, while for the field-testing point D3, the maximum acoustic pressure almost stayed the same; for the field-testing points D5-D8, the maximum acoustic pressures all clearly declined, and the maximum acoustic pressure at the field-testing point D5 reduced most with 4.68 dB, and the maximum acoustic pressures at the field-testing points D6-D8 reduced about 2.5 dB; for the field-testing points D9-D13, the maximum acoustic pressures at the field-testing points D9-D11, and D13 all declined, and reduced most at the field-testing point

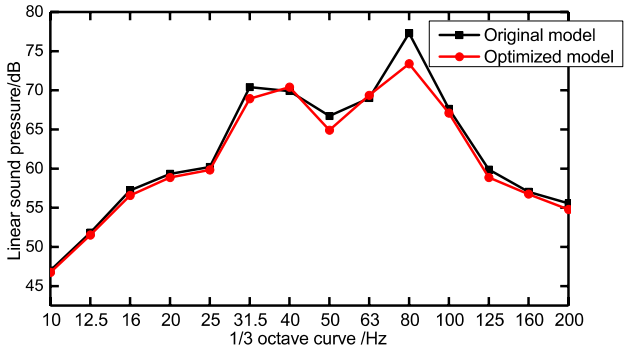

Fig. 16 Acoustic pressure spectrums for the optimized and raw models at field-testing point D9

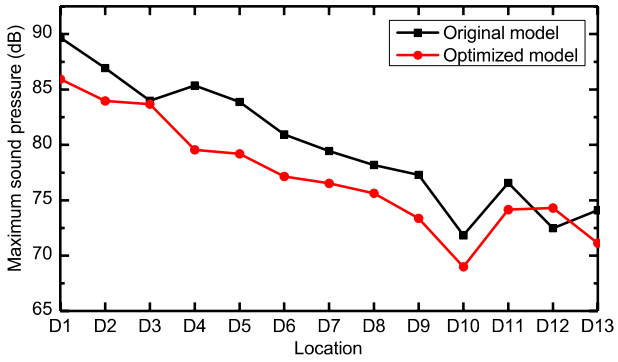

Fig. 17 The maximum acoustic pressures for each field-testing point

D9 with 3.93 dB, the maximum acoustic pressures at the field-testing points D10, D11 and D13 reduced about 2-3 dB, while the maximum acoustic pressure at the field-testing point D12 enlarged by 1.83 dB. Even the maximum acoustic pressures at certain testing point increased with limited amount, generally speaking, the maximum acoustic pressures at most field-testing points reduced obviously, which implies that the optimized model is capable of effectively mitigating the structure-borne noises in viaduct-like structures.

6. Conclusions

This study discussed the feasibility of application of MATV for connecting the vibration modes with the sound pressures in the structure-borne noise mitigation of viaduct box girder in HSR transportation system after modification for optimum structural performance improvement for alleviating the structure-borne noise, the acoustic sound pressure before and after acoustic field optimization are compared, and some conclusions can be summarized as follows:

As to the main frequency range, the structural dynamic vibration and structure-borne noise of the viaduct box girder both range within 100 Hz mainly, and also the dominant frequency bands both are [31.5, 80] Hz.

The 16^{th} and 62^{th} mode shapes serve as the main source in generating the structure-borne noise peak frequency for the viaduct box girder, and such two mode shapes primarily imply the local vibrations at the wing plate and the top plate.

In regards to the acoustic optimal design for the structure-borne noise, the introduction of rib plates at the position of the maximum amplitude of dominant mode shapes, the acoustic sound pressure shall be hereinafter evidently alleviated, and the structure-borne noise mitigation demonstration is superior to that of original design, which suggests potential application in real engineering.

Acknowledgement

This study is supported by National Natural Science Foundation of China (No. 51578238), and Jiangxi Advanced Scientific and Technological Innovation Team Project (No. 20152BCB24007).

References

Armentani, E., Caputo, F., Esposito, L., Giannella, V. and Citarella, R. (2018), "Multibody simulation for the vibration analysis of a turbocharged diesel engine", *Appl. Sci*., **8**(7), 1192. https://doi.org/10.3390/app8071192.

Armentani, E., Sbarbati, F., Perrella, M. and Citarella, R.G. (2016), "Dynamic analysis of a car engine valve train system", *J. Vehicle Noise Vib.*, **12**(3), 229-240. https://doi.org/10.1504/IJVNV.2016.080138.

Cao, H., Zhou, Y.L., Chen, Z. and Abdel Wahab, M. (2017), "Form-finding analysis of suspension bridges using an explicit iterative approach", *Struct. Eng. Mech.* **62**(1), 85-95. https://doi.org/10.12989/sem.2017.62.1.085.

Citarella, R., Federico, L., and Cicatiello, A. (2007), "Modal acoustic transfer vector approach in a FEM-BEM vibro-acoustic analysis", *Eng. Anal. Boundary Elements,* **31**, 248-258. https://doi.org/10.1016/j.enganabound.2006.09.004.

Crockett, A.R., and Pyke, J. (2000), "Viaduct Design for Minimization of Direct and Structure-radiated Train Noise", *J. Sound Vib.,* **231**(3), 883-897. https://doi.org/10.1006/jsvi.1999.2645.

Dai, W., Zheng, X., Luo, L., Hao, Z. and Qiu, Y. (2019), "Prediction of high-speed train full-spectrum interior noise using statistical vibration and acoustic energy flow", *Appl. Acoustics*, **145**, 205-219. https://doi.org/10.1016/j.apacoust.2018.10.010.

Dijckmans, A., Coulier, P., Jiang, J., Toward, M. G. R., Thompson, D. J., Degrande, G. and Lombaert, G. (2015), "Mitigation of railway induced ground vibration by heavy masses next to the track", *Soil Dynam. Earthq. Eng.*, **75**, 158-170. https://doi.org/10.1016/j.soildyn.2015.04.003.

Djojodihardjo, D. (2015), "Vibro-acoustic analysis of the acoustic-structure interaction of flexible structure due to acoustic excitation", *Acta Astronautcia*, **108**, 129-145. https://doi.org/10.1016/j.actaastro.2014.11.026.

Foglar, M. and Göringer, J. (2013), "Influence of the structural arrangement of bridges on the noise induced by traffic", *Eng. Struct.,* **56**, 642-655. https://doi.org/10.1016/j.engstruct.2013.05.039.

Gao, F., Xia, H., and An, N. (2010), "Analysis and experimental study on the radiation noise of the elevated structures of Beijing metro line 5", *China Railway Science,* **5**, 134-139.

Gerard, F., Tournour, M. and Masri, N.E. (2002), "Acoustic transfer vectors for numerical modeling of engine noise", *Sound*

Vib., **36**(7), 20-25.
Gille, LA., Favre, C.M. and Lam, K.C. (2017), "Partial and Total Annoyance Due to Road Traffic Noise Combined with Aircraft or Railway Noise: Structural Equation Analysis", *J. Environ. Res. Public Health,* **14**(1478), 1-18. https://doi.org/10.3390/ijerph14121478.
Han, J., Wu, D. and Li, Q. (2012), "Influence of deck thickness and stiffeners on structure-borne noise of the trough beams", *J. Vib. Eng*, **05**, 589-594.
Harari, A. and Sandman, B.E. (1990), "Radiation and vibration properties of submerged stiffened cylindrical shells", *J. Acoustical Soc. America,* **88**(4), 1817-1830. https://doi.org/10.1121/1.400203.
He, X., Wu, T., Zou, Y., Chen, Y. F., Guo, H. and Yu, Z. (2017), "Recent developments of high-speed railway bridges in China", *Struct. Infrastruct. Mech.*, **13**, 1584-1595. https://doi.org/10.1080/15732479.2017.1304429.
Kopuz, S., Unlusoy, Y.S. and Caliskan, M. (1996), "Integrated FEM/BEM approach to the dynamic and acoustic analysis of plate structures", *Eng. Anal. Boundary Elements,* **17**, 269-77. https://doi.org/10.1016/S0955-7997(96)00026-4.
Li, X., Zhang, X. and Liu, Q. (2013), "Prediction of structure-borne noise of high-speed railway bridges in whole frequency bands (part I): theoretical model", *J. China Railway Soc.,* **35**(01), 101-107.
Li, Q., Song, X. and Wu, D. (2014), "A 2.5-dimensional method for the prediction of structure-borne low-frequency noise from concrete rail transit bridges", *J. Acoustical Soc. America,* **135**(2718), 2718-2726. https://doi.org/10.1121/1.4871357.
Liang, L., Li, X., Yin, J., Wang, D., Gao, W. and Guo, Z. (2019), "Vibraiton characteristics of damping pad floating slab on the long-span steel truss cable-stayed in urban transit", *Eng. Struct.,* **191**, 92-103. https://doi.org/10.1016/j.engstruct.2019.04.032.
Liao, C., Jiang, W. and Wang, Y. (2009), "Vibration and acoustic radiation of axially stiffened finite cylindrical shells in water", *J. Vib. Shock,* **28**(5), 74-79.
Liu, G., Li, S., Li, Y. and Chen, H. (2013), "Vibration analysis of pipelines with arbitrary branches by absorbing transfer matrix method", *J. Sound Vib.,* **332**, 6519-6536. https://doi.org/10.1016/j.jsv.2013.06.019.
Liu, J. and Song, L. (2002), "Vibration and noise of the urban rail transit", *J. Traffic Transport. Eng*., **1**, 29-33.
Møller, H. and Pedersen, C.S. (2011), "Low-frequency noise from large wind turbines", *J. Acoustical Soc. America* **129**(6), 3727-3744. https://doi.org/10.1121/1.3543957.
Ngai, K.W. and Fng, C. (2002), "Structure-Borne Noise and Vibration of Concrete Box Structure and Rail Viaduct", *J. Sound Vib.,* **255**(2), 281-297. https://doi.org/10.1006/jsvi.2001.4155.
Quinn, D.D. (2012), "Modal analysis of jointed structures", *J. Sound Vib.,* **331**, 81-93. https://doi.org/10.1016/j.jsv.2011.08.017.
Sadri, M. and Younesian, D. (2015), "Vibro-acoustic analysis of a coach platform under random excitation", *Thin Wall. Struct.*, **95**, 287-296. https://doi.org/10.1016/j.tws.2015.07.008.
Siano, D., Citarella, R. and Armentani, E. (2018), "Simulation of the vibrational behaviour of a multi-cylinder engine", *J. Vehicle Noise Vib.* **14**(2), 101-123. https://doi.org/10.1504/IJVNV.2018.095158.
Takashima, R., Takiguchi, T. and Ariki, Y. (2013a), "Dimensional feature weighting utilizing multiple kernel learning for single-channel talker location discrimination using the acoustic transfer function", *J. Acoustical Soc. America,* **133**(891), 891-901. https://doi.org/10.1121/1.4773255.
Takashima, R., Takiguchiy, T. and Arikiz, Y. (2013b), "Single-channel talker localization based on separation of the acoustic transfer function using hidden Markov model and its classification", *Acoustic Sci. Technol.,* **34**(3), 176-186. https://doi.org/10.1250/ast.34.176.
Thota, M. and Wang, K.W. (2017), "Reconfigurable origami sonic barriers with tunable bandgaps for traffic noise mitigation", *J. Appl. Phys.*, **122**, 154901. https://doi.org/10.1063/1.4991026.
Waye, K.P. (2011), "Effects of Low Frequency Noise and Vibrations: Environmental and Occupational Perspectives", *Encyclopedia Environ. Health,* 240-253.
Werning, B.S., Beier, M. and Degen, K.G. (2001), "Research on noise and vibration reduction at DB to improve the environmental friendliness of railway traffic", *Revista De Biologia Tropical,* **49**(3), 1237-1252. https://doi.org/10.1016/j.jsv.2005.08.065.
Xie, W., Chen, X. and Pan, Z. (2008), "Analysis of acoustic radiation from rein-forced concrete cylindrical shell in air", *J. Noise Vib. Control,* **28**(3), 109-112.
Zhang, H., Xie, X., Jiang, J. and Yamashita, M. (2015a), "Assessment on transient sound radiation of a vibrating steel bridge due to traffic loading", *J. Sound Vib.,* **336**, 132-149. https://doi.org/10.1016/j.jsv.2014.10.006.
Zhang, X., Li, X. and Liu, Q.M. (2013a), "Theoretical and experimental investigation on bridge-borne noise under moving high-speed train", *Sci. China Technol. Sci.*, **56**(4), 917-924. https://doi.org/10.1007/s11431-013-5146-0.
Zhang, X., Li, X. and Liu, Q. (2013b), "Prediction of structure-borne noise of high-speed railway bridges in whole frequency bands (part II): field test verification", *J. China Railway Soc.,* **35**(02), 87-192.
Zhang, X., Zhang, J. and Li, X. (2015b), "Analysis of train-induced bridge vibration and noise based on beam-plate hybrid elements", *J. Noise Vib. Control*, **35**(01), 89-92.

CC

Nomenclature

$A(\omega)$	Modal acoustic transfer vector (MATV)
c	Sound speed in air
j	Imaginary part
f	Calculation frequency
i	i^{th} structural mode
L	Meshing size
N	Modes considered
p	Acoustic pressure
u	Structural displacement
v	Structural vibration velocity at the normal direction
ω	Circular frequency
Ω	Structural modal matrix
$\{MCF(\omega)\}$	Modal contribution factor
Ω_n	Sub-vector matrix at the normal direction of structural surface of the structural vibration modes
Subscripts	
s	s^{th} location
Superscripts	
T	Conjugate